

Understanding Changes in the Tropical Circulation under Global Warming Using a Cloud-Resolving Model and a Conceptual Model

SRAMANA NEOGI^{a,b} AND MARTIN S. SINGH^{a,b}

^a *School of Earth, Atmosphere and Environment, Monash University, Australia*

^b *ARC Centre of Excellence for Climate Extremes, Monash University, Australia*

(Manuscript received 29 October 2021, in final form 14 May 2022)

ABSTRACT: A cloud-resolving model (CRM) is used to investigate how a prototype tropical circulation driven by a sea surface temperature (SST) contrast changes in a warmer climate. The CRM is used to simulate a region of the atmosphere with a positive SST anomaly, and the large-scale circulation in this region is represented using the weak temperature gradient (WTG) and damped gravity wave (DGW) parameterizations, where the large-scale vertical velocity within the domain is related to the deviation of the simulated density profile from a reference profile representative of the tropical mean state. The behavior of the circulation in response to an increase in SST of both the domain and reference state (i.e., uniform warming) is examined. While the vertical velocity shows an increase in its maximum strength with warming, its value in the lower to midtroposphere decreases. Since the water vapor concentration is largest in the lower troposphere, this leads to a dynamic weakening of precipitation under warming. To understand these results, a simple model for the thermodynamic structure of a convecting atmosphere based on a bulk entraining plume is employed. The model uses a fixed entrainment rate and the relative humidity profiles from the CRM to predict the temperature profiles of the domain and reference state. The vertical velocity profiles calculated from these predicted temperature profiles reproduce important aspects of those simulated with the CRM. This simple modeling framework reveals that the effect of entrainment is crucial to understanding the dynamic response of precipitation to warming, providing a stepping stone to understanding the factors driving changes to the tropical precipitation distribution in a future warmer climate.

KEYWORDS: Atmospheric circulation; Cloud resolving models; Large-scale motions; Parameterization; Entrainment


1. Introduction

Differences in projections of regional precipitation among climate models have been the focus of a number of studies. A useful framework is to divide changes to regional precipitation in response to warming into two main components: a component associated with changes in atmospheric moisture content (the thermodynamic component; Held and Soden 2006; Chou and Neelin 2004) and a component associated with changes in circulation patterns (the dynamic component; e.g., Seager et al. 2010; Xie et al. 2015). While the thermodynamic component leads to a robust acceleration of the hydrological cycle under warming by enhancing the climatological pattern of precipitation minus evaporation (the “wet-gets-wetter” response; Held and Soden 2006), regional precipitation projections are dominated by changes owing to the dynamic component, which is strongly model dependent (Chadwick et al. 2013).

Previous authors have developed theories to help untangle the factors controlling the dynamic response of tropical precipitation to warming. For example, Chou and Neelin (2004) argued that a reduction in gross moist stability driven by increased low-level moisture could provide a dynamic amplification of the thermodynamic component. They termed this

combined dynamic–thermodynamic mechanism the “rich-get-richer” response. The authors also introduced an “upped-ante” mechanism, which tends to suppress precipitation in the convective margins due to advection of dry air from subsidence regions. The work of Chou and Neelin (2004) and a number of more recent studies (Chou et al. 2009; Levine and Boos 2016; Wills et al. 2017) applies a simplified representation of tropical dynamics in which the vertical velocity is assumed to follow a first-baroclinic mode structure. However, observational estimates of tropical vertical velocities differ from this simple structure; Back and Bretherton (2006) argued that the large-scale tropical overturning could be better represented through a combination of two modes with top- and bottom-heavy vertical motion profiles, respectively (Back and Bretherton 2009; Duffy et al. 2020).

An alternate approach is to focus on the role of surface conditions in driving large-scale circulations. In the tropics, the smallness of the Coriolis parameter prevents strong horizontal density gradients from being maintained (Charney 1963). This is the basis for the weak temperature gradient (WTG) approximation, which has been widely applied in modeling and theoretical studies of the tropical atmosphere (e.g., Sobel and Bretherton 2000; Sobel et al. 2001; Raymond and Zeng 2005). The WTG approximation combined with the assumption of convective quasi-equilibrium (QE), which suggests that precipitating regions of the tropics are constrained to remain close to moist convective neutrality, together imply that precipitation over tropical oceans is a strong function of surface temperature (Neelin and Held 1987). This has led some authors to argue that projected regional precipitation

 Denotes content that is immediately available upon publication as open access.

Corresponding author: Sramana Neogi, sramana.neogi@monash.edu

DOI: 10.1175/JCLI-D-21-0854.1

© 2022 American Meteorological Society. For information regarding reuse of this content and general copyright information, consult the AMS Copyright Policy (www.ametsoc.org/PUBSReuseLicenses).

changes over tropical oceans are closely related to changes in the pattern of sea surface temperature (SST) (Xie et al. 2010; Ma et al. 2012; Xie et al. 2015). For example, enhanced warming in equatorial regions has been associated with a contraction of seasonal precipitation toward the equator (Zhou et al. 2019). Over land regions, changes in humidity as well as temperature are important, but the importance of surface conditions in modulating future precipitation changes remains (Lambert et al. 2017; Todd et al. 2018).

In this paper, we aim to understand one component of the complex coupling between precipitation, SST patterns, and circulation changes. Specifically we investigate how a prototype tropical circulation driven by an SST contrast is affected by uniform warming. We use a simple modeling approach in which a cloud-resolving model (CRM) is coupled to a parameterized large-scale circulation using techniques based on the WTG approximation. The CRM domain is taken to be the ascending branch of the circulation, and the profile of large-scale ascent is determined based on the difference in the thermodynamic profile of the domain and that of a reference state representing the tropical mean. Two parameterizations are applied: the WTG parameterization proposed by Sobel and Bretherton (2000), in which large-scale ascent is assumed to relax the atmosphere toward the reference state, and the damped gravity wave (DGW) parameterization, in which the large-scale dynamics is simplified to a gravity wave with a single horizontal wavenumber (Kuang 2008a).

Previous studies using the WTG and DGW parameterizations have examined how the large-scale circulation responds to changes in local thermodynamic conditions such as the local SST, moisture, and wind speed within the ascending branch (Wang and Sobel 2011; Raymond and Zeng 2005; Daleu et al. 2017). Here, we examine changes in the circulation due to increases in the SST of the tropical-mean reference state in order to understand how the parameterized large-scale circulation behaves in a global warming scenario. A recent study by Saint-Lu et al. (2020) used a similar WTG approach to decompose the changes in precipitation in future GCM projections using a single-column model. Here we use a cloud-resolving approach, and we focus on understanding the fundamental interactions between convection and the large-scale circulation under warming.

To understand the changes in the parameterized large-scale circulation in the CRM, we apply a simple conceptual model for the temperature structure of the atmosphere introduced by Singh and O’Gorman (2013) and based on the assumption that convection maintains a lapse rate that is neutrally buoyant with respect to an entraining plume. According to this zero-buoyancy plume (ZBP) model, the effect of entrainment causes the ascent region to be more stable than the tropical-mean reference state, and this affects the vertical profile of the parameterized large-scale circulation. In particular, we find that entrainment causes the profile of vertical motion to become increasingly top-heavy with increasing SST, contributing to a dynamic weakening of precipitation within the ascent region under warming. The model therefore provides a framework for understanding how details of convective

mixing influence the large-scale circulation and its changes in a warming climate.

We begin by describing the CRM formulation, the implementation of the WTG and DGW parameterizations, and the results for precipitation and large-scale circulation (section 2). We then introduce the conceptual ZBP model and apply it to understand the simulations (section 3). Finally, we present a summary and our conclusions (section 4).

2. Cloud-resolving model simulations

a. Model specification

We conduct a series of simulations of the ascending branch of a steady large-scale circulation in the tropics using a cloud-resolving model, the System for Atmospheric Modeling (SAM; Khairoutdinov and Randall 2003). SAM solves the anelastic equations of motion, where the prognostic variables used are the three components of the vector velocity, liquid/ice static energy, and total precipitating and nonprecipitating water. Prognostic scalars are advected using the positive-definite scheme of Smolarkiewicz and Grabowski (1990). Radiation is parameterized using the Rapid Radiative Transfer Model (RRTM; Clough et al. 2005) and a single-moment microphysics scheme is used that treats hydrometeor partitioning as a function of temperature. Subgrid-scale turbulence is parameterized using a 1.5-order closure for turbulence kinetic energy.

We have prescribed a doubly periodic domain of $96 \text{ km} \times 96 \text{ km}$ with a horizontal grid spacing of 1 km. The vertical column is divided into 74 levels with an uneven spacing of 75 m near the surface and an even spacing of 500 m from 3 km to the model top, set at 33 km. Newtonian damping is applied in the top one-third of the model to prevent reflection of gravity waves. We have turned off the diurnal and seasonal cycle in the model and imposed a solar insolation of 551.58 W m^{-2} at the top of the atmosphere at a zenith angle of 42.05° . A lower boundary condition of uniform SST is imposed and surface turbulent fluxes are estimated using Monin–Obukhov similarity theory. The simulations are run for 100 days with a time step of 10 s and we have taken the last 50 days for analysis, after the model reaches a statistically steady state. All simulations are run with no rotation (Coriolis parameter $f = 0$).

b. Supra-domain-scale parameterizations

To couple the model to the large-scale circulation, we apply a set of methods referred to by Romps (2012) as supra-domain-scale (SDS) parameterizations. Two such methods are employed: the weak temperature gradient (WTG; Sobel and Bretherton 2000; Wang and Sobel 2011; Raymond and Zeng 2005) and damped gravity wave (DGW; Kuang 2008a) parameterizations. These parameterizations estimate the effects of the large-scale circulation using the fact that, in the tropics, the smallness of the Coriolis parameter prevents strong horizontal density gradients from being maintained in the troposphere (Charney 1963; Sobel and Bretherton 2000). Specifically, the profile of large-scale ascent is calculated by requiring that the modeled temperature (WTG) or pressure

(DGW) profile remains close to that of a reference state representative of the tropical mean. Our implementation of the WTG and DGW parameterizations is similar to previous CRM studies (Daleu et al. 2015; Raymond and Zeng 2005; Wang and Sobel 2011); a brief description of both the schemes is presented below.

1) WEAK TEMPERATURE GRADIENT PARAMETERIZATION

The WTG parameterization has several different formulations: the strict WTG method (Sobel and Bretherton 2000), the relaxed WTG method (Raymond and Zeng 2005), and the more recent spectral WTG method (Herman and Raymond 2014). In this paper, we follow a similar implementation to the relaxed WTG method proposed by Raymond and Zeng (2005). This method assumes that the large-scale circulation acts to relax the horizontal-mean temperature profile of the model domain to a specified reference state. Specifically, the domain-mean vertical velocity $\bar{w}(z)$ as a function of height z is given by

$$\bar{w}(z) = \sin\left(\pi \frac{z - z_b}{z_t - z_b}\right) \left[\frac{\bar{T}(z) - T_{\text{ref}}(z)}{\tau_{\text{WTG}} \partial_z \bar{s}} \right], \quad (1)$$

where $T(z)$ and $T_{\text{ref}}(z)$ are the temperatures of the domain and the reference state, respectively, z_t is the tropopause height, z_b is the height of the boundary layer, $\partial_z \bar{s}$ is the vertical gradient of dry static energy $s(z) = c_p T + gz$, with c_p being the isobaric specific heat capacity and g the gravitational acceleration, and the overbars indicate domain-mean quantities. Following Raymond and Zeng (2005), Wang and Sobel (2011), and Daleu et al. (2015), we set the time scale of relaxation $\tau_{\text{WTG}} = 3$ h.

According to Sobel and Bretherton (2000), the WTG approximation is invalid in the boundary layer, where turbulent fluxes develop buoyancy anomalies at a faster rate than the gravity waves can act to redistribute them. We therefore apply (1) in the free troposphere, between the top of the boundary layer $z_b = 1$ km and the tropopause z_t . Here z_t is defined as the level at which the lapse rate $\Gamma = -\partial_z T$ is equal to 2 K km^{-1} . Within the boundary layer, the vertical velocity is interpolated from its value at z_b to zero at the surface. Above the tropopause z_t , \bar{w} is set to zero. Further, we follow Raymond and Zeng (2005) in incorporating a height dependency to the efficiency with which the tropospheric relaxation occurs, represented by the sine function in (1), with the relaxation being most efficient in the midtroposphere. Finally, in order to prevent unrealistically large values of \bar{w} in the upper troposphere, the static stability is capped at 1 K km^{-1} ; that is, the value of $\partial_z \bar{s}$ in (1) is not allowed to decrease below 1 K km^{-1} . Although there is no theoretical justification for this 1 K km^{-1} limit, similar limits are applied in many previous implementations of the WTG method (e.g., Daleu et al. 2015; Raymond and Zeng 2005).

2) DAMPED GRAVITY WAVE PARAMETERIZATION

The DGW parameterization, originally formulated by Kuang (2008a), calculates the domain-mean vertical velocity by assuming that convection within the column interacts with a large-scale

gravity wave with a single horizontal wavenumber k . Using equations for momentum and hydrostatic balance under the anelastic approximation, Kuang (2008a) derived an evolution equation for the domain-mean vertical velocity under such conditions in terms of the domain-mean virtual temperature profile $\bar{T}_v(z)$ and the virtual temperature profile of a reference state $T_{v,\text{ref}}(z)$, representative of the tropical mean. Here, we are interested in the steady-state case, and we may therefore write the equation governing the domain-mean vertical velocity as

$$\frac{\partial}{\partial z} \left[\frac{1}{\tau_{\text{DGW}}} \frac{\partial(\bar{\rho} \bar{w})}{\partial z} \right] = -k^2 \bar{\rho} g \frac{\bar{T}_v - T_{v,\text{ref}}}{T_{v,\text{ref}}}, \quad (2)$$

where τ_{DGW} is a mechanical damping time scale, k is the horizontal wavenumber of the gravity wave, and $\bar{\rho}(z)$ is the domain-mean density profile. Following the work of Wang et al. (2013) and Daleu et al. (2015), we set $\tau_{\text{DGW}} = 1$ day and $k = 10^{-6} \text{ m}^{-1}$. Equation (2) is solved using Thomas' triangular matrix method with the boundary conditions of $\bar{w} = 0 \text{ m s}^{-1}$ at the surface and at the upper boundary z_u , which we set to 20 km. Note that this is different from the implementation of the WTG parameterization outlined in section 2b(1), where the upper limit is explicitly set by the tropopause height z_t . This is because the WTG method is not applicable in the stratosphere. The DGW method, on the other hand, is valid over the entire column, and we set the upper limit well above the tropopause to allow the model to produce its own structure in the tropopause region. Above z_u , $\bar{w}(z)$ is set to zero.

c. Simulations coupled to the parameterized large-scale circulation

To apply the SDS parameterizations described above, we must define the reference state temperature and virtual temperature profiles. To do so, we run the model to radiative-convective equilibrium (RCE) at a fixed SST. In RCE, the domain-mean vertical velocity $\bar{w}(z) = 0$, and the simulation develops a steady state in which radiative cooling balances convective heating. The domain- and time-mean temperature and virtual temperature profiles from this RCE simulation are used as the reference state. The model is then coupled to the SDS parameterization schemes described above (WTG or DGW) and the simulation is reinitialized from the reference state and with an increased SST. The parameterized large-scale vertical velocity $\bar{w}(z)$ advects water vapor and liquid/ice static energy vertically, introducing new sources and sinks in the model's moisture and energy budgets. This is incorporated by modifying the prognostic water vapor and thermodynamic equations at each time step to include an additional term as follows:

$$\frac{\partial q}{\partial t} = \dots - \bar{w} \frac{\partial \bar{q}}{\partial z}, \quad (3)$$

$$\frac{\partial h}{\partial t} = \dots - \bar{w} \frac{\partial \bar{h}}{\partial z}, \quad (4)$$

where q is the specific humidity, h is the liquid/ice static energy, and we evaluate the advective tendencies based on

domain-mean quantities, represented by the overbars. This implementation neglects horizontal moisture advection [termed *lateral entrainment* by Raymond and Zeng (2005)] into the domain from its surroundings, which has previously been accounted for by considering the inflow of moisture into the domain to be represented by the moisture profile of some prescribed environment (Sessions et al. 2010).

Since the reference state represents the tropical mean, we refer to the SST of the RCE simulations used to calculate the reference state as the background SST, while the difference between the SST imposed in the WTG/DGW simulations and that of the reference state is referred to as the relative SST (Wang and Sobel 2011). On physical grounds, we expect positive relative SSTs to correspond to large-scale ascent, and we therefore refer to the domain simulated by the WTG and DGW simulations as the ascent region. Our aim is to understand how the character of this large-scale ascending circulation varies with both relative and background SST.

We conduct a set of RCE simulations at five different background SSTs from 296 to 304 K in steps of 2 K. For each background SST, we consider four different relative SSTs, from 0 to 1.5 K in steps of 0.5 K. An increase in the background SST is analogous to the effects of uniform warming, while an increase in the relative SST is analogous to an enhancement of the existing SST pattern. Several studies have looked into the vertical velocity structures with changing relative SST (e.g., Wang and Sobel 2011). Here we emphasize the changes in vertical velocity structures with increasing background SST and their implications for precipitation within the ascent region.

d. Results

1) PARAMETERIZED VERTICAL VELOCITY

Figure 1 shows the parameterized large-scale vertical velocity profiles at different relative SSTs (0, 0.5, 1, and 1.5 K) at a background SST of 300 K. For a relative SST of 0 K, the SST is equal to that of the background reference state, and we would expect no large-scale circulation [Edman and Romps (2015) termed such cases “self-consistency tests”]. Indeed, for zero relative SST, the parameterized vertical velocity is small at all heights, suggesting that our RCE state is stable and provides a reasonable reference state.

For positive relative SSTs, the vertical velocity profile is positive through most of the troposphere, and its magnitude increases with increasing relative SST. Furthermore, in both the WTG and DGW cases, the parameterized vertical velocity profiles are top-heavy, with maxima at about 9 km above which they gradually decrease to zero at about 14 km. Similar results were seen in previous studies applying SDS parameterizations (Wang and Sobel 2011; Raymond and Zeng 2005; Daleu et al. 2015), while such top-heavy profiles were described by Back and Bretherton (2006) as characteristic of the vertical velocity profiles seen in the west Pacific warm pool region. Note that in the WTG case the tropopause was set at 14 km for a background SST of 300 K, and the vertical velocity is set to zero above this level. The DGW simulations show similar behavior in the upper troposphere even though the DGW

parameterization is applied up to the level $z_u = 20$ km. Analyzing the vertical velocity profiles for different relative SSTs at a fixed background SST allows us to verify that our model results are consistent with previous studies (e.g., Wang and Sobel 2011). As we will show below, however, the response to relative SST increases is qualitatively different to the response to background SST increases; it is the latter that is the main focus of this manuscript.

To explore how the large-scale circulation changes in response to uniform global warming, we compare the parameterized vertical velocity profiles for simulations at different background SSTs while keeping the relative SST fixed. Since the results are qualitatively similar for different relative SSTs, we focus on the case with a relative SST of 1 K (Fig. 2). As the background SST increases, the parameterized vertical velocity profiles become increasingly top-heavy, with the profile of the vertical velocity essentially shifting upward. These changes in shape can be seen more clearly by normalizing each profile by its maximum value (Figs. 2c and 2d). This upward-shift behavior is different to that seen in Fig. 1, where the shape of the vertical velocity profiles remain unchanged as the relative SST is increased. Wang and Sobel (2011) also observed relatively weak differences in the shape of the vertical velocity profile in their study of WTG-parameterized circulations at different relative SSTs. The increase in the top-heaviness of the $\bar{w}(z)$ profiles is thus a response of parameterized large-scale circulations to warming of the ascent region and reference state together (uniform warming) rather than a response to increases in relative SST (localized warming). Similar extensions of the vertical velocity profile have previously been attributed to a deeper troposphere as a result of warmer surface conditions (Tompkins and Craig 1999; Singh and O’Gorman 2012). Note however that the upward shift of the vertical velocity profiles seen in Fig. 2 persists even when the vertical coordinate is normalized by the tropopause height (not shown). This suggests that this upward shift is governed by not only the deepening of the troposphere, but that other factors also come into play.

In addition to an upward shift, the magnitude of the maximum vertical velocity also increases as the background SST is increased (Fig. 2). In combination, these effects lead to an increase in $\bar{w}(z)$ in the upper troposphere, but a decrease in the lower to middle troposphere in response to increasing background SST. For example, at a height of 3 km and for an increase in background SST from 298 to 300 K, the strength of the vertical velocity decreases by $0.06 \text{ cm s}^{-1} \text{ K}^{-1}$ for the WTG parameterization while for the DGW case it shows a decrease of about $0.3 \text{ cm s}^{-1} \text{ K}^{-1}$. As we shall see below, the magnitude of $\bar{w}(z)$ in the lower troposphere is particularly important for determining the domain-mean precipitation rate in the simulations.

2) NET SURFACE PRECIPITATION ($\bar{P}-\bar{E}$)

Changes in the large-scale circulation under warming lead to a “dynamic” contribution to precipitation changes in the tropics. To examine this in the context of our simulations, we performed a decomposition of the moisture budget equation

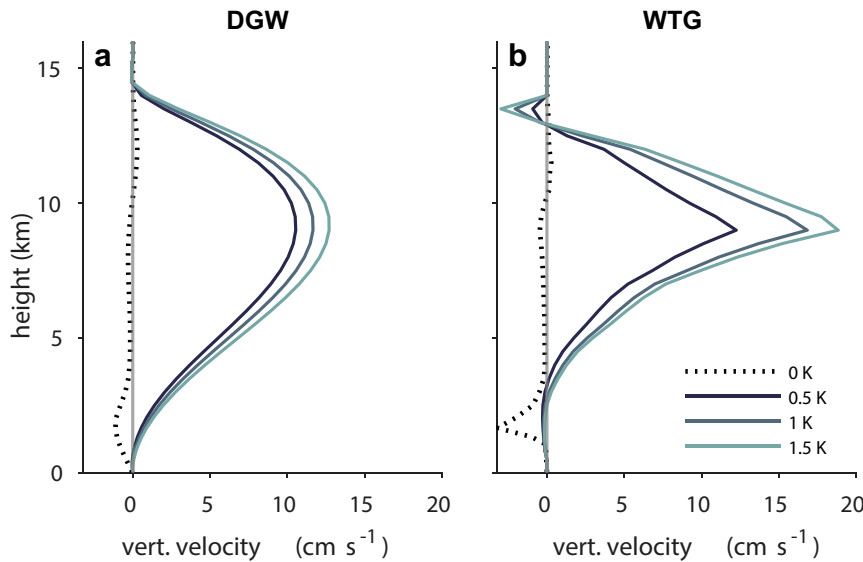


FIG. 1. Parameterized large-scale vertical velocity profiles $\bar{w}(z)$ at different relative SSTs (0, 0.5, 1, and 1.5 K) at fixed background SST of 300 K in CRM simulations using the (a) DGW and (b) WTG parameterizations.

to express the changes to the net precipitation rate, given by the domain-mean precipitation minus evaporation, into thermodynamic and dynamic components. Similar decompositions have been performed by a number of studies with slight differences in methodology depending on the application (e.g., Seager et al. 2010; Ma et al. 2012; Chou and Neelin 2004).

Integrating the moisture budget equation vertically and averaging over the model domain, we may relate the surface precipitation P and surface evaporation E to the vertical advection of specific humidity q by the parameterized large-scale circulation:

$$(\bar{P} - \bar{E}) = - \left\langle \bar{w} \frac{\partial \bar{q}}{\partial z} \right\rangle, \quad (5)$$

where $\langle X \rangle$ indicates a mass-weighted integration over the whole column and, as before, the overbar refers to a domain mean. Here $(\bar{P} - \bar{E})$ gives the net precipitation at the surface averaged over the model domain. Taking the differential of both sides of (5) and dividing by (5) allows us to write an approximate equation for the fractional changes in $(\bar{P} - \bar{E})$ with warming:

$$\frac{\delta(\bar{P} - \bar{E})}{(\bar{P} - \bar{E})} = \frac{\left\langle (\delta \bar{w}) \frac{\partial \bar{q}}{\partial z} \right\rangle}{\left\langle \bar{w} \frac{\partial \bar{q}}{\partial z} \right\rangle} + \frac{\left\langle \bar{w} \frac{\partial}{\partial z} (\delta \bar{q}) \right\rangle}{\left\langle \bar{w} \frac{\partial \bar{q}}{\partial z} \right\rangle}. \quad (6)$$

Here, δX refers to a difference between simulations at successive background SSTs for fixed relative SST, and we have neglected terms that involve the product of such differences.

The first term on the right-hand side of (6) gives the dynamic component of the fractional change in $(\bar{P} - \bar{E})$, and it

depends on changes in the circulation $\delta \bar{w}$. The second term gives the thermodynamic component, and it depends on changes in moisture $\delta \bar{q}$.

Figure 3 shows the three terms in (6) for both the WTG and DGW parameterization schemes and across the range of background SSTs simulated. While we expect the sum of the thermodynamic component (green bars) and dynamic component (yellow bars) to be roughly equal to the change in net precipitation (blue bars), higher-order terms neglected in (6) also contribute. These neglected terms reach a magnitude of up to 17.4% of the thermodynamic component. Notwithstanding this nonlinearity, it may be seen that in most cases the net precipitation rate $(\bar{P} - \bar{E})$ increases with warming, and this increase is a result of a competition between a positive thermodynamic component and a negative dynamic component. The thermodynamic component has a magnitude ranging from 13.6% to 15.6% K^{-1} for the WTG simulations and from 7.9% to 8.5% K^{-1} for the DGW simulations across the range of background SSTs simulated. In previous studies, the thermodynamic component has been found to roughly follow the fractional increase of near-surface saturation specific humidity with warming (Held and Soden 2006), which for typical tropical surface temperatures is around 7% K^{-1} . While the DGW simulations are consistent with this expectation, the thermodynamic increase in $(\bar{P} - \bar{E})$ in the WTG simulations is substantially larger. This is because the expression for the thermodynamic component involves an integral of the fractional change of the vertical specific humidity gradient weighted by the vertical velocity profile. For the WTG case, $\bar{w}(z)$ is strongly upper troposphere amplified, and the thermodynamic component follows the higher fractional increase of moisture in the upper troposphere. While the profile of $\bar{w}(z)$ in the DGW simulations is

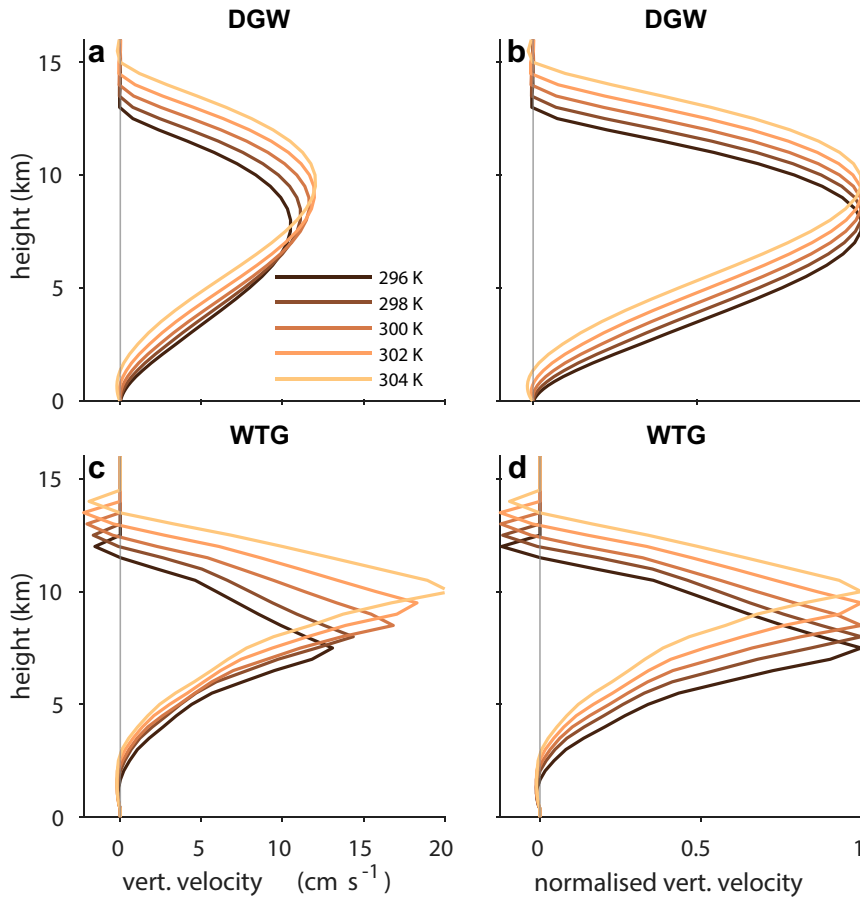


FIG. 2. Profiles of (a),(c) parameterized large-scale vertical velocity $\bar{w}(z)$ and (b),(d) vertical velocity normalized by its maximum value at different background SSTs as labeled in (a) with fixed relative SST of 1 K in CRM simulations using the (top) DGW and (bottom) WTG parameterizations.

also top-heavy, it still has substantial weight in the lower troposphere, leading to a value of the thermodynamic component closer to the fractional increase in surface saturation specific humidity.

For both the WTG and DGW cases, the dynamic component is negative across the range of background SSTs simulated. This may initially be surprising because the magnitude of the maximum of $\bar{w}(z)$ increases monotonically with background SST. But it may be explained by noting that the fractional changes of $\bar{w}(z)$ are weighted by the vertical gradient of specific humidity in the expression for the dynamic component. In our CRM simulations, and in the tropics more generally, humidity and its vertical gradient are largest near the surface, where the vertical velocity decreases with warming [Fig. 2; for a background SST of 300 K, the maximum $\partial_z \bar{q} = -2.94 \text{ g kg}^{-1} \text{ km}^{-1}$ occurs at a height of 500 m (not shown), where the change in vertical velocity with warming is $\delta \bar{w} = -0.1 \text{ cm s}^{-1} \text{ K}^{-1}$]. Thus, understanding the profile of the large-scale vertical velocity and its changes with warming is of vital importance for understanding the effect of large-scale dynamics on precipitation changes in our simulations.

3) TEMPERATURE

The large-scale vertical velocity parameterized by the WTG and DGW methods is governed by the temperature difference between the ascent region and the reference state. According to the WTG parameterization, $\bar{w}(z)$ depends directly on the difference between the temperature of the domain and the reference state via (1). In the DGW parameterization, $\bar{w}(z)$ is governed by the difference in virtual temperatures of the domain and the reference state through an elliptic partial differential equation. In both cases, the temperature anomaly $\Delta T(z) = \bar{T} - T_{\text{ref}}$ plays a key role in determining the parameterized vertical velocity profile. Although this relationship is straightforward for the WTG parameterization, it is somewhat harder to intuit for the DGW parameterization. This is because temperature anomalies at a particular level affect the vertical velocity over the whole column via (2). A Green's function analysis shows that, for the DGW parameterization, the influence of a perturbation in $\Delta T(z)$ at a given level decreases linearly with distance from the value at that level to zero at the surface and at $z_u = 20 \text{ km}$. This Green's function is independent of the parameters τ_{DGW} and k .

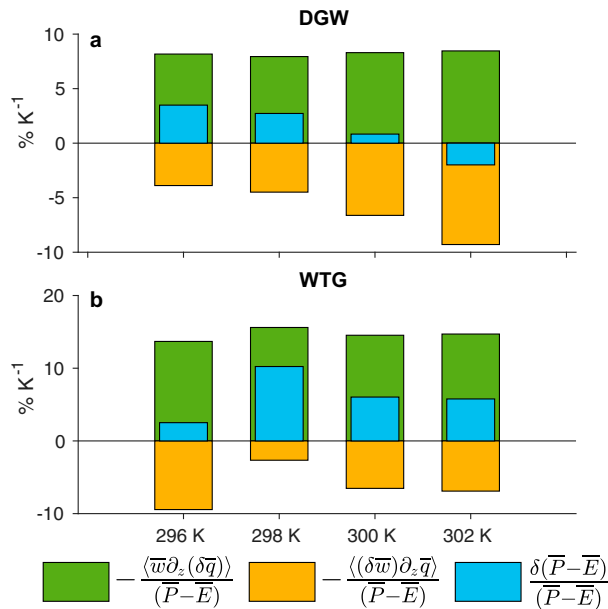


FIG. 3. Fractional rate of change in net precipitation ($\bar{P} - \bar{E}$) with increasing background SST (blue) broken into thermodynamic (green) and dynamic (yellow) components in CRM simulations using the (a) DGW and (b) WTG parameterizations. Rates are estimated by taking differences between simulations with background SSTs as labeled and simulations with background SSTs 2 K higher, all at a fixed relative SST of 1 K.

Figures 4a and 4b show that the temperature anomaly $\Delta T(z)$ simulated by the CRM is negative in the lower troposphere for both the WTG and DGW cases. This implies that the domain is cooler than the reference state in the lower troposphere, despite the fact that the SST is higher in the domain than in the reference state. In both cases, ΔT gradually increases with height, becoming positive in the midtroposphere and reaching a maximum near the tropopause. The temperature anomalies also show a decrease in the lower to midtroposphere and a stronger upper-troposphere amplification with warming. Since the profile of $\Delta T(z)$ is directly related to the top-heaviness of the vertical velocity profile $\bar{w}(z)$, understanding the changes in vertical velocity with background SST requires an understanding of the temperature profiles of both the ascent region and the reference state. In the next section, we use a simple conceptual model for the thermal structure of the atmosphere to explore the factors controlling $\Delta T(z)$ in our CRM simulations. Based on this, we will use (1) and (2) to investigate the implications for the vertical velocity profile $\bar{w}(z)$.

3. Zero buoyancy plume model

a. Model description

A common assumption in theoretical studies of the tropical circulation is that the lapse rate of the atmosphere remains close to that of a moist adiabat (e.g., Neelin and Zeng 2000;

Emanuel 2007; Levine and Boos 2016). Indeed, observational studies suggest that moist convective neutrality is a reasonable first-order approximation for the tropical mean state (Xu and Emanuel 1989). However, both modeling (Singh and O’Gorman 2013) and observational (Schiro and Neelin 2019) evidence is accumulating that the tropical tropospheric temperature deviates from that associated with an undilute parcel ascent (i.e., a moist adiabat) and instead is better represented by the temperature of a rising air parcel that entrains environmental air.

To account for the effects of entrainment on the tropical thermal structure, Singh and O’Gorman (2013) developed the zero-buoyancy plume (ZBP) model in which convection is represented by an entraining plume that is assumed to remain neutrally buoyant with respect to the environment. Singh and O’Gorman (2013) used the ZBP model to provide a simple estimate of the thermal structure of the atmosphere in RCE. Here, we will use it to estimate the temperature profiles $\bar{T}(z)$ and $T_{\text{ref}}(z)$ simulated by the CRM. As shown in Figs. 4a and 4b, the free-tropospheric temperature within clouds in our CRM simulations is close to that of the domain mean, justifying the use of the ZBP model.

As shown by Romps (2014), the assumption of neutrality with respect to an entraining plume allows one to write an approximate equation for the lapse rate $\Gamma = -\partial_z T$ within the troposphere given by

$$\Gamma = \Gamma_m + \frac{\epsilon L_v q_{\text{sat}} (1 - \mathcal{R})}{c_p \left(1 + \frac{L_v^2 q_{\text{sat}}}{c_p R_v T^2} \right)}, \quad (7)$$

where

$$\Gamma_m = \left(\frac{g}{c_p} \right) \frac{1 + \frac{q_{\text{sat}} L_v}{R_d T}}{1 + \frac{q_{\text{sat}} L_v^2}{c_p R_v T^2}} \quad (8)$$

is the moist adiabatic lapse rate, T and q_{sat} are the temperature and saturation specific humidity, respectively, of both the plume and the environment at a given level, ϵ is the fractional rate of entrainment of environmental air into the plume, \mathcal{R} is the relative humidity of the environment, and R_d and R_v are the gas constants for dry air and water vapor, respectively. Here we have neglected virtual effects so that the ZBP assumption amounts to the assumption of equal temperature in the plume and its environment. Given the relative humidity, temperature, and pressure at a given level, (7) gives the lapse rate as a function of the entrainment rate ϵ . According to (7), the key factors controlling the deviation of the lapse rate from moist adiabatic are the saturation deficit of the environment $q_{\text{sat}}(1 - \mathcal{R})$ and the entrainment rate ϵ . As the environment approaches saturation or the rate of entrainment decreases, Γ becomes smaller, resulting in a more stable troposphere [$\Gamma \rightarrow \Gamma_m$ when $q_{\text{sat}}(1 - \mathcal{R}) \rightarrow 0$ and $\epsilon \rightarrow 0$].

For a given profile of relative humidity $\mathcal{R}(z)$, the ZBP model may be used to derive the full temperature profile in

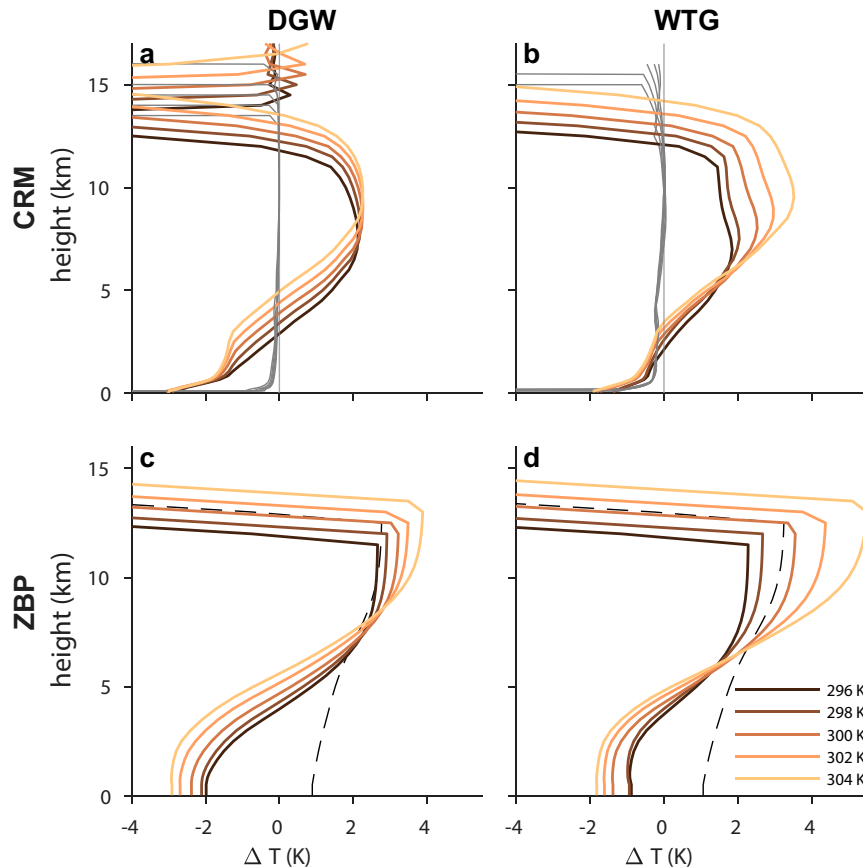


FIG. 4. Profiles of temperature anomaly $\Delta T(z)$ for the (a),(b) CRM and (c),(d) ZBP model and for the (left) DGW and (right) WTG parameterizations. Lines correspond to parameterizations at different background SSTs as labeled in (d) with a fixed relative SST of 1 K. Gray lines in (a) and (b) represent the temperature difference between in-cloud temperatures (the mean temperature of grid points with at least 0.01 g kg^{-1} of cloud water/ice) and domain-mean temperatures. The black dotted line in (c) and (d) is the $\Delta T(z)$ profile in the ZBP model for a background SST of 300 K and zero entrainment ($\epsilon = 0 \text{ K}^{-1}$).

the following way. First, a midtropospheric level is chosen at a height z_0 , with temperature T_0 and pressure p_0 . We then integrate (7) and the equation for hydrostatic balance downward to the cloud base [here taken as $z_{\text{LCL}} = 500 \text{ m}$, roughly representing the lifting condensation level (LCL)] and upward to the tropopause, above which an isothermal stratosphere is imposed. The integration is performed using the fourth-order Runge–Kutta method with a variable step size, given by the spacing of the vertical grid in the CRM. Below the LCL, the temperature is determined by assuming constant dry static energy.

To apply the ZBP model to the CRM results presented in the previous section, we choose the level $z_0 = 7 \text{ km}$, and we take the relative humidity profile $\mathcal{R}(z)$, temperature T_0 , and pressure p_0 at $z = z_0$ as being given by the time- and domain-mean variables output from the corresponding CRM simulations. The choice of the reference level ($z_0 = 7 \text{ km}$) is made such that $\Delta T(z)$ at $z = z_0$ is set in the midtroposphere. This is motivated by the observation that, in the CRM simulations, the temperature anomalies maximize in the midtroposphere

(Figs. 4a and 4b) and govern the strength of the vertical velocity. We further set the tropopause to be the level at which the temperature is equal to the temperature at the tropopause in the corresponding CRM simulation. Finally, we set the entrainment rate ϵ by comparing the time- and domain-mean lapse rate from an RCE simulation with the CRM at an SST of 300 K with the lapse rate predicted by the ZBP model using (7). We use a range of entrainment rates ($\epsilon = 0$ to 1 km^{-1} at intervals of 0.1 km^{-1}) and use the $\mathcal{R}(z)$ and T_0 from the CRM simulation at RCE. We choose $\epsilon = 0.7 \text{ km}^{-1}$ based on the agreement between the lapse rates simulated with the CRM and given by the ZBP model in the lower troposphere (not shown).

With the above procedure, we may use the ZBP model to provide estimates of the temperature profiles $\bar{T}(z)$ and $T_{\text{ref}}(z)$ corresponding to the mean profiles of the ascent region and the reference state for the different combinations of relative and background SST simulated with the CRM. Based on these profiles, we may calculate the temperature anomaly

$\Delta T(z)$, and by applying (1) and (2) we may also derive ZBP model-based estimates of the large-scale vertical velocity profile $\bar{w}(z)$ for each case shown in the previous section. Consistent with the neglect of virtual effects above, we replace virtual temperatures with temperatures in (2) when calculating the vertical velocity. Below we compare these estimates to the results of the CRM, and we use the ZBP model to interpret the physical processes driving the changes in $\bar{w}(z)$ with increasing background SST.

b. Results

We begin by comparing the temperature anomaly profiles $\Delta T(z)$ from the ZBP model to those of the CRM simulations. As seen in Fig. 4, the simulated profiles of $\Delta T(z)$ are relatively well reproduced by the ZBP model. In both cases, $\Delta T(z)$ is negative in the lower troposphere for both the WTG and DGW parameterizations and gradually increases with height to a maximum just below the tropopause (Fig. 4). The negative values of $\Delta T(z)$ near the surface are unexpected given that the temperature anomaly at z_0 , imposed by setting T_0 in the ZBP model, is positive. As mentioned in the previous section, near-surface values of $\Delta T < 0$ indicate that the boundary layer of the ascent region is cooler than the reference state.

To examine the factors that control $\Delta T(z)$ in the ZBP model, we use (7) to write an approximate expression for its vertical gradient $\partial_z \Delta T$:

$$\begin{aligned} \frac{\partial \Delta T}{\partial z} &= \Gamma_{\text{ref}} - \Gamma \\ &= \Gamma_{m,\text{ref}} - \Gamma_m + \frac{\epsilon L_v q_{\text{sat}} (\mathcal{R} - \mathcal{R}_{\text{ref}})}{c_p \left(1 + \frac{L_v^2 q_{\text{sat}}}{c_p R_v T^2} \right)}, \end{aligned} \quad (9)$$

where the subscript “ref” gives a variable evaluated in the reference state; for ease of interpretation, we have neglected the temperature difference between the ascent region and the reference state in the last term on the right-hand side. According to (9), the vertical gradient of $\Delta T(z)$ is controlled by two effects: an effect owing to the temperature dependence of the moist adiabatic lapse rate (first two terms on the right-hand side) and the effect of entrainment, which depends on the difference in environmental humidity between the ascent region and the reference state (last term on the right-hand side). If entrainment is set to zero, the profile of $\Delta T(z)$ is determined by the temperature dependence of the moist adiabatic lapse rate, and it increases by a factor of roughly 3 from the lower troposphere to the upper troposphere (Figs. 4c,d). The profile of $\Delta T(z)$ with entrainment set to zero is very similar to the temperature anomaly profiles derived by Yu and Neelin (1997) under the assumption of convective quasi-equilibrium. When entrainment is included, however, the lapse rate depends also on the relative humidity. Since the simulated relative humidity profiles are provided as input to the ZBP model, and since $\mathcal{R}(z)$ (represented by the WTG/DGW simulations) is higher than $\mathcal{R}_{\text{ref}}(z)$ (represented by the RCE simulations) (Fig. 5a), the lapse rate is more stable in the ascent region than in the reference state. As a result, the temperature anomaly $\Delta T(z)$ increases even more strongly with height, and this leads to

negative values of $\Delta T(z)$ at low levels. The ability of the ZBP model to reproduce the CRM-simulated $\Delta T(z)$ profiles provides confidence that this physical explanation is relevant to the CRM.

As the background SST is increased, the profiles of $\Delta T(z)$ become more amplified in the upper troposphere according to both the CRM and ZBP models (Fig. 4). Once again, this may be understood by examining (9). As the atmosphere warms, the saturation specific humidity q_{sat} increases, causing the effect of entrainment on the lapse rate to become larger (Singh and O’Gorman 2013), and thereby causing $\partial_z \Delta T$ to increase. Variations in the relative humidity difference $\mathcal{R} - \mathcal{R}_{\text{ref}}$ with warming (Figs. 5b and 5c) modulate this increase, but calculations of the ZBP model with the relative humidity profiles fixed to their value at a background SST of 300 K (not shown) indicate that this is a minor effect. We may therefore conclude that, for the ZBP model, the variation in the shape of $\Delta T(z)$ with background SST is primarily a result of the increase in the tropospheric saturation deficit with warming following the Clausius–Clapeyron relation, which leads to an increase in the effect of entrainment on the lapse rate of a neutrally buoyant plume.

Figure 6 replots the vertical velocity profiles simulated by the CRM, originally shown in Figs. 2a and 2b, and compares them to those predicted by the ZBP model for both the DGW and WTG parameterizations. The ZBP model reproduces a number of key features of the CRM-simulated vertical velocity profiles and their behavior with increased background SST, including their top-heavy structure and the “upward shift” of the profiles with warming. Specifically, the ZBP model reproduces the increase in the maximum value of $\bar{w}(z)$ and concurrent decrease in $\bar{w}(z)$ at low levels seen in the CRM simulations with increasing background SST. For the DGW case, the ZBP model predicts downward motion [$\bar{w}(z) < 0$] at low levels for the highest SSTs; this is qualitatively consistent with the CRM simulations, although for the ZBP model the strength of the descent is sensitive to the treatment of the tropopause. In the case shown, the ZBP model substantially overestimates the strength of the CRM-simulated large-scale descent. But if the tropopause in the ZBP model is set based on the height of the tropopause in the corresponding CRM simulation z_t (rather than its temperature), this overestimation is reduced. Notwithstanding this sensitivity, these results highlight the utility of the ZBP model for understanding the factors controlling the future changes to large-scale tropical circulations.

As described previously, the vertical velocity profile $\bar{w}(z)$ is determined largely by the temperature anomaly profile $\Delta T(z)$, which according to the ZBP model is strongly influenced by entrainment. To quantify the effect of entrainment on the vertical velocity profile, we compare our results for the ZBP model above with the special case of $\epsilon = 0 \text{ km}^{-1}$. When entrainment is neglected, the lapse rate of the plume remains equal to the moist adiabatic lapse rate ($\Gamma = \Gamma_m$) and no longer depends on the environmental humidity. In this case, the profiles of $\bar{w}(z)$ do not show a decrease with warming in the lower troposphere in either of the DGW and WTG parameterizations (Figs. 6e and 6f), contrary to the behavior of the ZBP model with entrainment included and the behavior

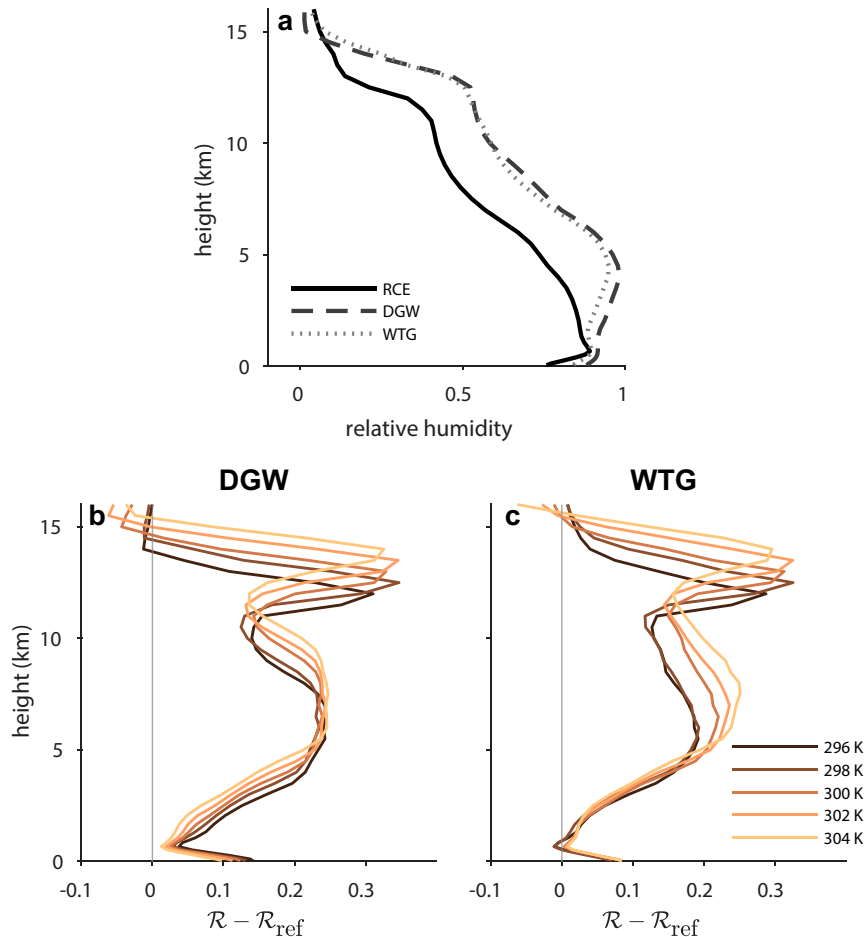


FIG. 5. (a) CRM-simulated relative humidity profiles for the RCE reference state with a background SST of 300 K and the corresponding DGW and WTG cases with a relative SST of 1 K. Difference between relative humidity profiles in the CRM simulations using the (b) DGW and (c) WTG parameterizations compared to those of the reference state at different background SSTs as labeled and with a fixed relative SST of 1 K.

of the CRM simulations. Given the importance of the low-level vertical velocity in the decomposition of net precipitation presented in section 2d, this suggests that convective entrainment may play an important role in determining precipitation responses to future global warming.

The above results may be understood in the following way. When entrainment is set to zero, the ZBP model predicts an upward shift of the vertical velocity profile with warming following a deepening troposphere, but the vertical velocity at low levels is largely unchanged. However, when entrainment is included, the increased saturation deficit in the troposphere leads to a temperature anomaly profile $\Delta T(z)$ that becomes more positive in the upper troposphere and more negative in the lower troposphere. This, in turn, leads to an increase in top-heaviness of the vertical velocity profile (including a decrease in vertical velocity at low levels) through the WTG and DGW parameterizations.

A limitation of the ZBP model is that it overestimates the peak magnitude of the vertical velocities, particularly for the

WTG parameterization. This is related to an overestimation of the temperature anomaly $\Delta T(z)$ in the upper troposphere (Fig. 4), which by (1) leads to an overestimation of $\bar{w}(z)$ at these levels. A likely reason for this overestimation is that the ZBP approximation fails in the upper troposphere, where the assumption of convective neutrality is less well justified (Kuang 2008b; Tulich and Mapes 2010). Despite this caveat, the simple ZBP model has been shown to replicate key results from our idealized CRM simulations, including some of the effects of uniform warming on the profile of large-scale ascent. This suggests the potential utility of the ZBP model for analyzing large-scale tropical circulations under more realistic conditions (e.g., in global climate models).

4. Summary and discussion

We have used a simple modeling technique to investigate how tropical large-scale circulations coupled to convection behave in a warming climate. A cloud-resolving model (CRM)

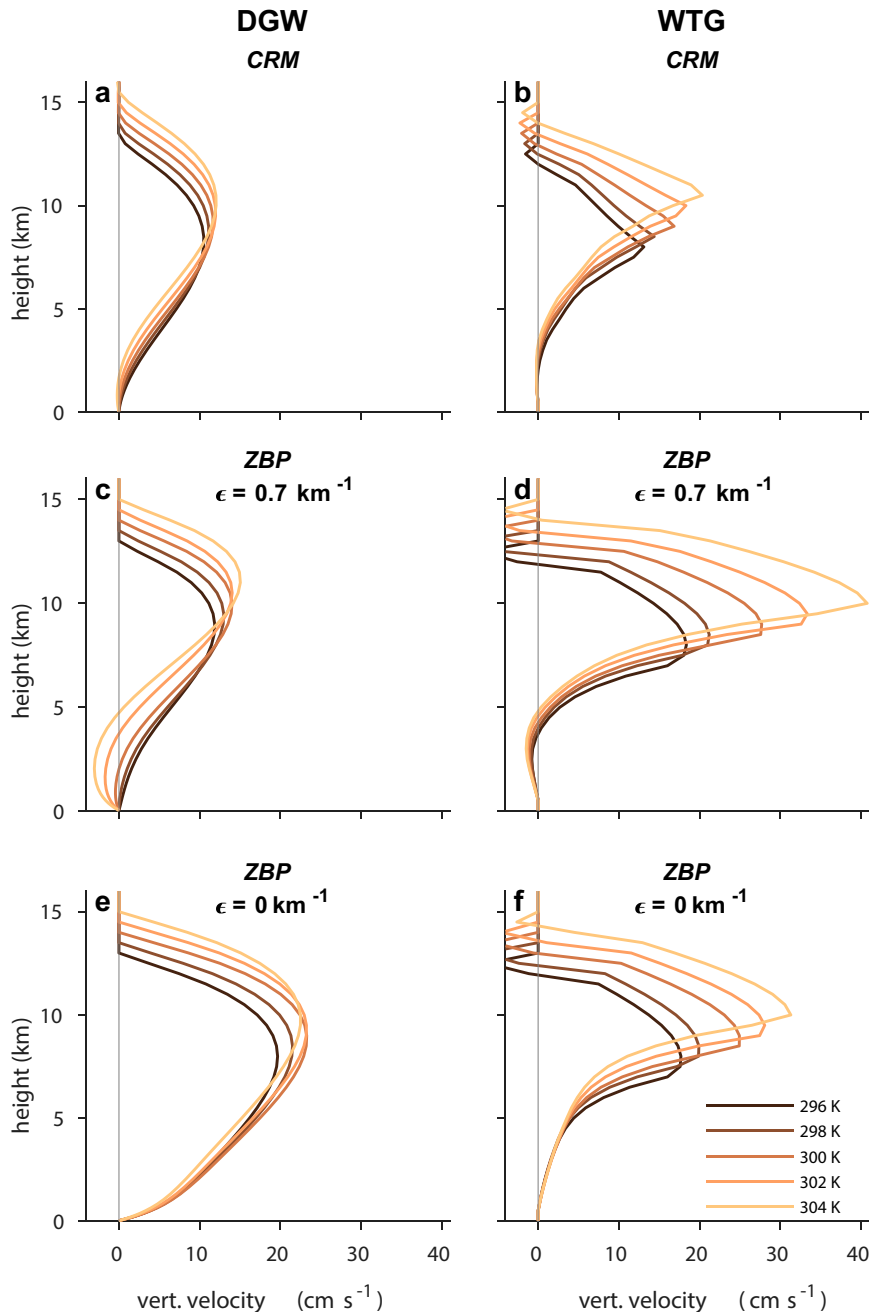


FIG. 6. Profiles of parameterized large-scale vertical velocity $\bar{w}(z)$ according to the (a),(b) CRM and (c)–(f) ZBP models at different background SSTs as labeled with a fixed relative SST = 1 K for the (left) DGW and (right) WTG parameterizations. Here, (c) and (d) show profiles with positive entrainment ($\epsilon = 0.7 \text{ km}^{-1}$), and (e) and (f) show profiles with zero entrainment ($\epsilon = 0 \text{ km}^{-1}$).

is used to simulate the ascending region of such a circulation in which the model domain is assumed to have a higher SST than that of a reference state representing the tropical mean. The profile of large-scale ascent is then parameterized by the weak temperature gradient (WTG) and damped gravity wave (DGW) methods. A number of studies have used this technique to examine changes in the parameterized circulation as

the SST in the domain is increased relative to that of the reference state (localized warming; e.g., Wang and Sobel 2011; Daleu et al. 2012; Raymond and Zeng 2005). Our purpose is to use the same framework to study the changes in the vertical velocity of the ascent region due to an equal increase in the SST of the domain and the reference state (uniform warming). We found that, while the magnitude of the peak vertical

velocity increases with warming, the strength of the ascent in the lower to midtroposphere decreases with warming. This translates to a negative dynamic contribution to changes in net precipitation (precipitation minus evaporation) in the ascent region because the vertical gradient of specific humidity is highest near the surface and decreases with height. These results lead us to conclude that the nature of the large-scale vertical velocity profile and its behavior under warming are crucial when considering dynamic contributions to changes in precipitation.

In the WTG and DGW parameterization schemes, the vertical velocity is related to the temperature difference between the ascending column and the reference state. This allowed us to use a simple model of tropical temperature profiles based on the assumption of neutrality with respect to an entraining plume to help understand the simulated changes in vertical velocity. According to this zero-buoyancy plume model, the effect of entrainment causes the lapse rate within the troposphere to decrease with the environmental relative humidity. In the simulations, the ascent region is moister than the background reference state, and this leads to a temperature anomaly profile that increases with height, and ultimately a top-heavy vertical velocity profile.

As the atmosphere warms, the effect of entrainment increases with the saturation specific humidity (Singh and O’Gorman 2013), and this helps to explain the increase in the top-heaviness of the simulated vertical velocity profiles under warming. In particular, we showed that the effect of entrainment was key to understanding the decreases in the large-scale vertical velocity at low levels coupled with the increase in the vertical velocity at upper levels with warming. These low-level decreases in the vertical velocity profile drive the dynamic response of net precipitation to warming; when the ZBP model was run without entrainment, no such decreases were found.

When entrainment is set to zero, the ZBP model assumes moist adiabatic lapse rates within the troposphere, and the model has some similarities to the theory of quasi-equilibrium (QE) dynamics that has been used in a number of previous studies of the tropical atmosphere (Neelin and Zeng 2000; Levine and Boos 2016; Wills et al. 2017; Emanuel 2007). In the QE framework, the vertical velocity profile is represented by a single first-baroclinic mode structure function; we show in a companion paper that this structure function is closely related to the solution for \bar{w} obtained by setting $\epsilon = 0$ in the ZBP model (Singh and Neogi 2022). The importance of entrainment in our results therefore points to possible limitations of the QE framework for estimating future changes in regional precipitation.

Despite its ability to qualitatively reproduce the results of the CRM simulations, the ZBP model results differ quantitatively from those of the CRM in important ways. For example, in the DGW simulations, the ZBP model predicts downward motion in the lower troposphere of larger magnitude than the CRM. These negative vertical velocities are associated with negative temperature anomalies that arise in this region. The appearance of negative temperature anomalies is surprising in itself (given the positive temperature

forcing applied in both models), and it is not consistent with observed overturning circulations, in which the ascending branch tends to occur where the boundary layer is anomalously warm and moist (Nie et al. 2010). Nevertheless, such negative temperature anomalies are simulated by the CRM, albeit of smaller magnitude than predicted by the ZBP model. Sensitivity analysis suggests that, for the case of the ZBP model, the strength of the lower-tropospheric downward motion depends on the height to which the convective plume extends through the definition of tropopause. Further investigation of this sensitivity is left for future study.

The ZBP model also overestimates the magnitude of the peak vertical velocity, particularly in the WTG simulations. This is likely related to the failure of the assumptions of the ZBP model in the upper troposphere (Kuang 2008b), where the maximum in vertical velocity occurs. Another limitation of our implementation of the ZBP model is that we have considered the entrainment rate to be fixed both in height and with surface temperature. More realistic implementations might use an entrainment rate dependent on height, or a more sophisticated multiplume model with a spectrum of entrainment rates (Zhou and Xie 2019). In principle, the rate of entrainment may also be affected by warming; investigating this possibility is an important avenue for future work.

In this work, the ZBP model takes as an input the relative humidity from the CRM simulations. Previous studies have extended the ZBP model to allow for a prediction of the relative humidity in the setting of RCE (Romps 2014) and with a specified vertical velocity profile (Singh et al. 2019; Romps 2021). In an accompanying work, the authors develop a closed model of the thermodynamic and dynamic structure of a region of large-scale ascent by applying the model of Singh et al. (2019) and coupling it to the large-scale vertical velocity using the WTG/DGW parameterization methods (Singh and Neogi 2022).

The weak temperature gradient and damped gravity wave parameterization methods are based on the approximation of negligible horizontal temperature gradients in the tropics due to redistribution of buoyancy anomalies by gravity waves. These methods have been used extensively to represent large-scale circulations in limited area models in both idealized (Sobel and Bretherton 2000; Wang and Sobel 2011; Raymond and Zeng 2005; Daleu et al. 2015, 2012, 2017) and realistic (Wang et al. 2016) configurations. However, there remain limitations in the ability of such SDS parameterizations to capture the full response of the atmosphere to global warming. For example, Saint-Lu et al. (2020) found that a single-column model coupled to the WTG and DGW parameterizations could reproduce important features of the precipitation response of the parent general circulation model (GCM) to global warming. However, the single-column model failed to capture an overall weakening of the circulation found in most GCM projections (Knutson and Manabe 1995; Ma et al. 2012), and the authors attributed this to a lack of interaction between ascent and descent regions when the circulation is parameterized. This limitation may also account for why the peak vertical velocity in our simulations increases with warming,

in apparent disagreement with GCM projections of tropical circulation strength (Knutson and Manabe 1995).

To capture the remote interactions between the different components of the large-scale circulation, the entire circulation must be resolved. Formulations like the mock-Walker cell (Kuang 2012), in which an SST gradient is imposed on a long-channel domain, provide a possible avenue to explore the effects of uniform warming on large-scale tropical circulations in a more complete, yet suitably simple, framework. Studies of such formulations provide a potential stepping stone toward understanding the tropical circulation in its full complexity.

Acknowledgments. We acknowledge the financial support from the Australian Research Council through the Centre of Excellence for Climate Extremes (CE170100023), Grant DE190100866 and Grant DP200102954, and computational resources and services from the National Computational Infrastructure (NCI). We thank Tristan Abbott and two anonymous reviewers for comments that helped improve the manuscript.

Data availability statement. Simulation data and codes used in this work are available from the Monash Bridges repository at <https://doi.org/10.26180/20381580.v2>.

REFERENCES

- Back, L. E., and C. S. Bretherton, 2006: Geographic variability in the export of moist static energy and vertical motion profiles in the tropical Pacific. *Geophys. Res. Lett.*, **33**, L17810, <https://doi.org/10.1029/2006GL026672>.
- , and —, 2009: A simple model of climatological rainfall and vertical motion patterns over the tropical oceans. *J. Climate*, **22**, 6477–6497, <https://doi.org/10.1175/2009JCLI2393.1>.
- Chadwick, R., I. Boutle, and G. Martin, 2013: Spatial patterns of precipitation change in CMIP5: Why the rich do not get richer in the tropics. *J. Climate*, **26**, 3803–3822, <https://doi.org/10.1175/JCLI-D-12-00543.1>.
- Charney, J. G., 1963: A note on large-scale motions in the tropics. *J. Atmos. Sci.*, **20**, 607–609, [https://doi.org/10.1175/1520-0469\(1963\)020<0607:ANOLSM>2.0.CO;2](https://doi.org/10.1175/1520-0469(1963)020<0607:ANOLSM>2.0.CO;2).
- Chou, C., and J. D. Neelin, 2004: Mechanisms of global warming impacts on regional tropical precipitation. *J. Climate*, **17**, 2688–2701, [https://doi.org/10.1175/1520-0442\(2004\)017<2688:MOGWIO>2.0.CO;2](https://doi.org/10.1175/1520-0442(2004)017<2688:MOGWIO>2.0.CO;2).
- , —, C.-A. Chen, and J.-Y. Tu, 2009: Evaluating the “rich-get-richer” mechanism in tropical precipitation change under global warming. *J. Climate*, **22**, 1982–2005, <https://doi.org/10.1175/2008JCLI2471.1>.
- Clough, S. A., M. W. Shephard, E. J. Mlawer, J. S. Delamere, M. J. Iacono, K. Cady-Pereira, S. Boukabara, and P. D. Brown, 2005: Atmospheric radiative transfer modeling: A summary of the AER codes. *J. Quant. Spectrosc. Radiat. Transfer*, **91**, 233–244, <https://doi.org/10.1016/j.jqsrt.2004.05.058>.
- Daleu, C. L., S. J. Woolnough, and R. S. Plant, 2012: Cloud-resolving model simulations with one- and two-way couplings via the weak temperature gradient approximation. *J. Atmos. Sci.*, **69**, 3683–3699, <https://doi.org/10.1175/JAS-D-12-058.1>.
- , and Coauthors, 2015: Intercomparison of methods of coupling between convection and large-scale circulation: 1. Comparison over uniform surface conditions. *J. Adv. Model. Earth Syst.*, **7**, 1576–1601, <https://doi.org/10.1002/2015MS000468>.
- , R. S. Plant, and S. J. Woolnough, 2017: Using the weak-temperature gradient approximation to evaluate parameterizations: An example of the transition from suppressed to active convection. *J. Adv. Model. Earth Syst.*, **9**, 2350–2367, <https://doi.org/10.1002/2017MS000940>.
- Duffy, M. L., P. A. O’Gorman, and L. E. Back, 2020: Importance of Laplacian of low-level warming for the response of precipitation to climate change over tropical oceans. *J. Climate*, **33**, 4403–4417, <https://doi.org/10.1175/JCLI-D-19-0365.1>.
- Edman, J. P., and D. M. Romps, 2015: Self-consistency tests of large-scale dynamics parameterizations for single-column modeling. *J. Adv. Model. Earth Syst.*, **7**, 320–334, <https://doi.org/10.1002/2014MS000378>.
- Emanuel, K., 2007: Quasi-equilibrium dynamics of the tropical atmosphere. *The Global Circulation of the Atmosphere*, T. Schneider and A. H. Sobel, Eds., Princeton University Press, 186–218.
- Held, I. M., and B. J. Soden, 2006: Robust responses of the hydrological cycle to global warming. *J. Climate*, **19**, 5686–5699, <https://doi.org/10.1175/JCLI3990.1>.
- Herman, M. J., and D. J. Raymond, 2014: WTG cloud modeling with spectral decomposition of heating. *J. Adv. Model. Earth Syst.*, **6**, 1121–1140, <https://doi.org/10.1002/2014MS000359>.
- Khairoutdinov, M. F., and D. A. Randall, 2003: Cloud resolving modeling of the ARM summer 1997 IOP: Model formulation, results, uncertainties, and sensitivities. *J. Atmos. Sci.*, **60**, 607–625, [https://doi.org/10.1175/1520-0469\(2003\)060<0607:CRMOTA>2.0.CO;2](https://doi.org/10.1175/1520-0469(2003)060<0607:CRMOTA>2.0.CO;2).
- Knutson, T. R., and S. Manabe, 1995: Time-mean response over the tropical Pacific to increased CO₂ in a coupled ocean-atmosphere model. *J. Climate*, **8**, 2181–2199, [https://doi.org/10.1175/1520-0442\(1995\)008<2181:TMROTT>2.0.CO;2](https://doi.org/10.1175/1520-0442(1995)008<2181:TMROTT>2.0.CO;2).
- Kuang, Z., 2008a: Modeling the interaction between cumulus convection and linear gravity waves using a limited-domain cloud system-resolving model. *J. Atmos. Sci.*, **65**, 576–591, <https://doi.org/10.1175/2007JAS2399.1>.
- , 2008b: A moisture-stratiform instability for convectively coupled waves. *J. Atmos. Sci.*, **65**, 834–854, <https://doi.org/10.1175/2007JAS2444.1>.
- , 2012: Weakly forced mock Walker cells. *J. Atmos. Sci.*, **69**, 2759–2786, <https://doi.org/10.1175/JAS-D-11-0307.1>.
- Lambert, F. H., A. J. Ferraro, and R. Chadwick, 2017: Land-ocean shifts in tropical precipitation linked to surface temperature and humidity change. *J. Climate*, **30**, 4527–4545, <https://doi.org/10.1175/JCLI-D-16-0649.1>.
- Levine, X. J., and W. R. Boos, 2016: A mechanism for the response of the zonally asymmetric subtropical hydrologic cycle to global warming. *J. Climate*, **29**, 7851–7867, <https://doi.org/10.1175/JCLI-D-15-0826.1>.
- Ma, J., S.-P. Xie, and Y. Kosaka, 2012: Mechanisms for tropical tropospheric circulation change in response to global warming. *J. Climate*, **25**, 2979–2994, <https://doi.org/10.1175/JCLI-D-11-00048.1>.
- Neelin, J. D., and I. M. Held, 1987: Modeling tropical convergence based on the moist static energy budget. *Mon. Wea. Rev.*, **115**, 3–12, [https://doi.org/10.1175/1520-0493\(1987\)115<0003:MTCBOT>2.0.CO;2](https://doi.org/10.1175/1520-0493(1987)115<0003:MTCBOT>2.0.CO;2).
- , and N. Zeng, 2000: A quasi-equilibrium tropical circulation model—Formulation. *J. Atmos. Sci.*, **57**, 1741–1766,

- [https://doi.org/10.1175/1520-0469\(2000\)057<1741:AQETCM>2.0.CO;2](https://doi.org/10.1175/1520-0469(2000)057<1741:AQETCM>2.0.CO;2).
- Nie, J., W. R. Boos, and Z. Kuang, 2010: Observational evaluation of a convective quasi-equilibrium view of monsoons. *J. Climate*, **23**, 4416–4428, <https://doi.org/10.1175/2010JCLI3505.1>.
- Raymond, D. J., and X. Zeng, 2005: Modelling tropical atmospheric convection in the context of the weak temperature gradient approximation. *Quart. J. Roy. Meteor. Soc.*, **131**, 1301–1320, <https://doi.org/10.1256/qj.03.97>.
- Romps, D. M., 2012: Numerical tests of the weak pressure gradient approximation. *J. Atmos. Sci.*, **69**, 2846–2856, <https://doi.org/10.1175/JAS-D-11-0337.1>.
- , 2014: An analytical model for tropical relative humidity. *J. Climate*, **27**, 7432–7449, <https://doi.org/10.1175/JCLI-D-14-00255.1>.
- , 2021: Ascending columns, WTG, and convective aggregation. *J. Atmos. Sci.*, **78**, 497–508, <https://doi.org/10.1175/JAS-D-20-0041.1>.
- Saint-Lu, M., R. Chadwick, F. H. Lambert, M. Collins, I. Boutle, M. Whittall, and C. Daleu, 2020: Influences of local and remote conditions on tropical precipitation and its response to climate change. *J. Climate*, **33**, 4045–4063, <https://doi.org/10.1175/JCLI-D-19-0450.1>.
- Schiro, K. A., and J. D. Neelin, 2019: Deep convective organization, moisture vertical structure, and convective transition using deep-inflow mixing. *J. Atmos. Sci.*, **76**, 965–987, <https://doi.org/10.1175/JAS-D-18-0122.1>.
- Seager, R., N. Naik, and G. A. Vecchi, 2010: Thermodynamic and dynamic mechanisms for large-scale changes in the hydrological cycle in response to global warming. *J. Climate*, **23**, 4651–4668, <https://doi.org/10.1175/2010JCLI3655.1>.
- Sessions, S. L., S. Sugaya, D. J. Raymond, and A. H. Sobel, 2010: Multiple equilibria in a cloud-resolving model using the weak temperature gradient approximation. *J. Geophys. Res. Atmos.*, **115**, D12110, <https://doi.org/10.1029/2009JD013376>.
- Singh, M. S., and P. A. O’Gorman, 2012: Upward shift of the atmospheric general circulation under global warming: Theory and simulations. *J. Climate*, **25**, 8259–8276, <https://doi.org/10.1175/JCLI-D-11-00699.1>.
- , and —, 2013: Influence of entrainment on the thermal stratification in simulations of radiative-convective equilibrium. *Geophys. Res. Lett.*, **40**, 4398–4403, <https://doi.org/10.1002/grl.50796>.
- , and S. Neogi, 2022: On the interaction between moist convection and large-scale ascent in the tropics. *J. Climate*, **35**, 4417–4435, <https://doi.org/10.1175/JCLI-D-21-0717.1>.
- , R. A. Warren, and C. Jakob, 2019: A steady-state model for the relationship between humidity, instability, and precipitation in the tropics. *J. Adv. Model. Earth Syst.*, **11**, 3973–3994, <https://doi.org/10.1029/2019MS001686>.
- Smolarkiewicz, P. K., and W. W. Grabowski, 1990: The multidimensional positive definite advection transport algorithm: Nonoscillatory option. *J. Comput. Phys.*, **86**, 355–375, [https://doi.org/10.1016/0021-9991\(90\)90105-A](https://doi.org/10.1016/0021-9991(90)90105-A).
- Sobel, A. H., and C. S. Bretherton, 2000: Modeling tropical precipitation in a single column. *J. Climate*, **13**, 4378–4392, [https://doi.org/10.1175/1520-0442\(2000\)013<4378:MTPIAS>2.0.CO;2](https://doi.org/10.1175/1520-0442(2000)013<4378:MTPIAS>2.0.CO;2).
- , J. Nilsson, and L. M. Polvani, 2001: The weak temperature gradient approximation and balanced tropical moisture waves. *J. Atmos. Sci.*, **58**, 3650–3665, [https://doi.org/10.1175/1520-0469\(2001\)058<3650:TWTGAA>2.0.CO;2](https://doi.org/10.1175/1520-0469(2001)058<3650:TWTGAA>2.0.CO;2).
- Todd, A., M. Collins, F. H. Lambert, and R. Chadwick, 2018: Diagnosing ENSO and global warming tropical precipitation shifts using surface relative humidity and temperature. *J. Climate*, **31**, 1413–1433, <https://doi.org/10.1175/JCLI-D-17-0354.1>.
- Tompkins, A. M., and G. C. Craig, 1999: Sensitivity of tropical convection to sea surface temperature in the absence of large-scale flow. *J. Climate*, **12**, 462–476, [https://doi.org/10.1175/1520-0442\(1999\)012<0462:SOTCTS>2.0.CO;2](https://doi.org/10.1175/1520-0442(1999)012<0462:SOTCTS>2.0.CO;2).
- Tulich, S. N., and B. E. Mapes, 2010: Transient environmental sensitivities of explicitly simulated tropical convection. *J. Atmos. Sci.*, **67**, 923–940, <https://doi.org/10.1175/2009JAS3277.1>.
- Wang, S., and A. H. Sobel, 2011: Response of convection to relative sea surface temperature: Cloud-resolving simulations in two and three dimensions. *J. Geophys. Res. Atmos.*, **116**, D11119, <https://doi.org/10.1029/2010JD015347>.
- , —, and Z. Kuang, 2013: Cloud-resolving simulation of TOGA-COARE using parameterized large-scale dynamics. *J. Geophys. Res. Atmos.*, **118**, 6290–6301, <https://doi.org/10.1002/jgrd.50510>.
- , —, and J. Nie, 2016: Modeling the MJO in a cloud-resolving model with parameterized large-scale dynamics: Vertical structure, radiation, and horizontal advection of dry air. *J. Adv. Model. Earth Syst.*, **8**, 121–139, <https://doi.org/10.1002/2015MS000529>.
- Wills, R. C., X. J. Levine, and T. Schneider, 2017: Local energetic constraints on Walker circulation strength. *J. Atmos. Sci.*, **74**, 1907–1922, <https://doi.org/10.1175/JAS-D-16-0219.1>.
- Xie, S.-P., C. Deser, G. A. Vecchi, J. Ma, H. Teng, and A. T. Wittenberg, 2010: Global warming pattern formation: Sea surface temperature and rainfall. *J. Climate*, **23**, 966–986, <https://doi.org/10.1175/2009JCLI3329.1>.
- , and Coauthors, 2015: Towards predictive understanding of regional climate change. *Nat. Climate Change*, **5**, 921–930, <https://doi.org/10.1038/nclimate2689>.
- Xu, K.-M., and K. A. Emanuel, 1989: Is the tropical atmosphere conditionally unstable? *Mon. Wea. Rev.*, **117**, 1471–1479, [https://doi.org/10.1175/1520-0493\(1989\)117<1471:JTACU>2.0.CO;2](https://doi.org/10.1175/1520-0493(1989)117<1471:JTACU>2.0.CO;2).
- Yu, J.-Y., and J. D. Neelin, 1997: Analytic approximations for moist convectively adjusted regions. *J. Atmos. Sci.*, **54**, 1054–1063, [https://doi.org/10.1175/1520-0469\(1997\)054<1054:AAFMC>2.0.CO;2](https://doi.org/10.1175/1520-0469(1997)054<1054:AAFMC>2.0.CO;2).
- Zhou, W., and S.-P. Xie, 2019: A conceptual spectral plume model for understanding tropical temperature profile and convective updraft velocities. *J. Atmos. Sci.*, **76**, 2801–2814, <https://doi.org/10.1175/JAS-D-18-0330.1>.
- , —, and D. Yang, 2019: Enhanced equatorial warming causes deep-tropical contraction and subtropical monsoon shift. *Nat. Climate Change*, **9**, 834–839, <https://doi.org/10.1038/s41558-019-0603-9>.